

Fluxon transmission measurements of engineered long Josephson junctions for efficient computing

Han Cai, Liuqi Yu, Ryan Clarke, Waltraut Wustmann, and Kevin D. Osborn

Abstract—Single-Flux Quantum (SFQ) digital logic is typically both energy efficient and fast, but the logic that uses reversibility provides the most extreme method for improving efficiency. We are studying engineered long Josephson junctions (LJJs) that are components for future ballistic logic gates within a logic family named Reversible Fluxon Logic (RFL). Therein, the bit states are represented by two possible polarities of an SFQ. Here we test engineered LJJs with component JJ critical currents of $7.5 \mu\text{A}$ and a Josephson penetration depth of approximately 2.4 unit cells. In our study, the SFQ rest energy in the Long JJ is determined to be 47 zJ (regardless of bit state). The LJJs were tested in two environments, at 4.2 K in a helium dunk probe (DP) and 3.5 K in a cryogen-free refrigerator (CFR). The on-chip circuit consists of three parts in sequence: an SFQ launcher, the LJJ under test, and a detector that uses biased $20 \mu\text{A}$ JJs. Data show that SFQ detection events are synchronous with SFQ launch events in both setups, indicating possible ballistic SFQ transmission in the LJJs. The jitter of the events in the CFR setup indicates that we are limited by signal filtering in our CFR setup and by noise in the DP setup.

Index Terms—Single Flux Quantum, Long Josephson Junctions, Low-Energy Fluxon, Ballistic Reversible Logic, Energy Efficiency

I. INTRODUCTION

THE size and number of computations are increasing steadily and, consequently, there is a growing need to study the energy efficiency of computing. Novel circuits provide alternatives in computing methods, and provide insight into new computation, aside from the advantage of scaling down dimensions as is done by industry for complementary metal-oxide-semiconductor (CMOS) logic. As an example, the power consumption of an exascale computer with CMOS circuits will be more than 20 MW [1], and this supercomputer requires a significant infrastructure for cooling to room temperature such that various alternative technologies must be investigated. Superconducting single flux quantum (SFQ) digital logic offers fundamentally different computational approaches than CMOS. SFQ circuits contain Josephson junctions and in research-grade demonstrations can enable higher operational speed and lower power consumption than CMOS logic [14]. In addition, SFQ logic is closely related to Josephson voltage-standard technologies [2], [3] and has been applied to various applications, including digital receivers [4], internet network

switches [5], astronomical sensor readouts [6], [10], and qubit control [11], [13].

The most developed SFQ logic is irreversible [15]–[18], but reversible logic offers the highest energy efficiency in a given system of materials. Physically reversible gates have the potential to significantly reduce energy costs, and with new material processes, they can bring the energy cost per gate operation below $\ln(2)k_B T$. This is the entropy limit, known as Landauer’s limit, imposed for an irreversible gate with one bit of erasure. It is also comparable to the energy scale of thermal equilibrium $k_B T$, which relates to thermally induced errors in logic gates.

Previous demonstrations of reversible logic used adiabatically supplied power, including the negative-inductance SQUID (nSQUID) [19] and the reversible version of the adiabatic quantum flux parametron (R-AQFP) [20]. The nSQUID has been demonstrated with a DC bias to propel bits forward [21]. In contrast, AQFP is AC powered and normally demonstrated without logical reversibility, but it reportedly realizes an average energy cost of 1.4 zJ per gate operation [22] at 4.2 K. R-AQFP (a reversible AQFP) gate operation has been demonstrated [23] and simulations show that this can reach below Landauer’s limit in energy cost as one lowers the clock speed [25]. Despite the success of AQFP, the AC power required contains multiple phases, which creates design complexity compared to DC-powered logic types, including Rapid Single-Flux-Quantum (RSFQ) logic and variants.

One may instead use ballistic bits for reversible logic as an alternative to adiabatically powered types [26]–[29]. This type uses SFQ in long Josephson junctions (LJJs) as bit states in and out of the gates. The SFQ may also be called fluxons (or flux solitons) in our LJJs due to their spatially extended nature and solitonic properties within the LJJ. Related to this, in Reversible-fluxon logic (RFL) we have discovered in simulation a novel nonlinear resonance between pairs of LJJs to realize gate operations [26]. The most fundamental gate operation with this resonance is the NOT or inversion gate, which reverses the fluxon’s polarity and reaches an energy efficiency over 97 %. Furthermore, from simulations, we developed a CNOT gate [27] and a class of gates named asynchronous ballistic shift registers [28]. In other work, abstract models are explored for 3-terminal ballistic gates, which might later be built from LJJs [29], [30]. They are logically universal for computing if combined with a simpler 2-terminal gate.

In this study, we designed engineered LJJs as potential components of future RFL gates, measured transmission through the LJJs, and analyzed the results. The engineered

H. Cai and L. Yu are with the Quantum Material Center and the Department of Physics at the University of Maryland, College Park, MD 20742 USA

R. Clarke and W. Wustmann are with the Laboratory for Physical Sciences, University of Maryland, College Park, MD 20740 USA

K. D. Osborn is with the Laboratory for Physical Sciences, University of Maryland, College Park, MD 20740 USA, and the Joint Quantum Institute and Quantum Materials Center, University of Maryland, College Park, MD 20742 USA (email: kosborn@umd.edu)

LJJs contained undamped Josephson junctions (JJs) and our analysis shows that we are likely limited in loss by the discrete metamaterial LJJ design (made from multiple cells). To test the transmission through LJJs we use a fluxon launcher circuit before the LJJ and a fluxon detector circuit after the LJJ. We tested LJJ transmission at 4.2 K in a helium dunk probe (DP) and at 3.5 K in a cryogen-free refrigerator (CFR).

II. EXPERIMENT AND RESULTS

The engineered LJJs under test are designed to be later integrated into RFL gates. For a reliable design of circuits, we have formulated our LJJs using component inductors and JJs in a quasi-lumped metamaterial design. In this design, our Josephson penetration depth extends over two unit cells, where a unit cell is the periodic unit of the engineered LJJ. We study the LJJs using two chips and two experimental setups: helium dunk probe setup (DP) and cryogen-free refrigerator setup (CFR). Specifically, the two measurement setups provide different noise environments for our low-energy fluxons and circuits.

A. LJJ parameters, component analysis, and launch speed

Circuits in this work were fabricated utilizing $Nb/AlO_x/Nb$ trilayer Josephson junctions and other elements at a superconducting digital foundry (see acknowledgment). The main circuit in this work allows us to study fluxons traveling through our LJJs. The circuit consists of a DC-to-SFQ (DC/SFQ) converter that functions as a fluxon launcher, an LJJ, and an SFQ-to-DC (SFQ/DC) converter that functions as a fluxon detector. The detector circuit outputs measurable DC levels which transition upon arrival of a fluxon (see Fig. 1). A fluxon will be launched into the LJJ at every rising edge of an input waveform fed into our DC/SFQ converter (launcher). The SFQ/DC converter (detector) uses a T flip-flop (TFF) to switch between two states upon each fluxon arrival [32]. As a result, every edge corresponds to a fluxon arrival, and the detector output frequency should be half of the launcher input frequency.

Fig. 1 (A) and (B) depict a schematic and photographs of the test LJJ and surrounding test circuits. The left enlarged view in Fig. 1 (B) illustrates discrete LJJ cells consisting of niobium trilayer Josephson junctions (JJs) and interconnecting linear inductors. Inductor wires have an extracted inductance of $L/2 = 3.92$ pH per rail per cell (L per cell). In total, there are 79 cells in the LJJ circuit between the converters, with one JJ per cell. The critical current used in this paper is calculated from the designed current density, which has an unknown accuracy in the fabrication process. The nominal critical current density, J_c , is $1 \mu A/\mu m^2$, and the nominal JJ area per LJJ cell is $7.5 \mu m^2$. Consequently, the nominal critical current of the JJ in LJJs is $7.5 \mu A$. The unshunted JJ inductance, $L_J = \Phi_0/2\pi I_C$, is 43.88 pH. Thus, the ratio of inductance between the JJ and linear inductor L_J/L is 5.64 . The LJJ length is approximately $1300 \mu m$, which is significantly longer than the Josephson penetration depth ($\lambda_J = a\sqrt{L_J/L} \approx 14 \mu m$).

We determine the connecting linear inductance $L/2$ by measuring the SQUID self-inductance, which is fabricated

on the same wafer as our LJJ chip (in the same fabrication process). By analyzing the characteristics of SQUID voltage versus directly injected flux bias current (I_{fl}), we determine the self-inductance as $L_s = \Phi_0/\Delta I_{fl}$. Since the SQUID has the same linewidth as the narrowest wire in the rails of our LJJ, we can expect the inductance per length in the long narrow wire of the LJJ rails to be similar. The SQUID-measured inductance per length is 0.654 pH/ μm at a 3.8% standard deviation (see Appendix on SQUID measurements for details) for our $2 \mu m$ wide inductor wires. The cell size in this chip is $a = 6 \mu m$. Thus, the linear connecting inductance is $L/2 = 3.92$ pH.

Theoretically, the fluxon may lose energy from discreteness as it moves through the LJJ, resulting in the emission of plasma waves [33]. However, in our structures we expect the energy loss and related velocity change to be small [26], [34]. For example, in previous experimental structures [34], a typical discreteness parameter used was $a/\lambda_J = \sqrt{1/7}$. With a small ratio of a/λ_J , we can consider the discreteness as negligible in single gate simulations [26]. The ratio used in this paper is $\sqrt{1/5.64}$. However, our simulation indicates the fluxon moves nearly ballistically even under this ratio. Using the nominal critical currents and the extracted inductances, we simulated the SFQ generation and launch process. Our simulations give a launch velocity of $v \approx 0.78c$. This velocity is higher than the initial velocity we usually use in simulating gates $v = 0.6c$ (where c is the Swihart velocity [?]), and experimentally it is even possible that the fluxon will stop within the LJJ.

B. Measurement of converters and LJJs with the DP setup

Before testing the LJJs, we conducted tests of converters without LJJs. The test circuit for this includes a DC/SFQ converter, which generates an SFQ from every input DC pulse, and an SFQ/DC converter, which signals the arrival of an SFQ pulse. A $100 \mu A$ -JTL section is used to connect these two converters. The chip schematic is shown in Fig. 2 (A). In one measurement setup, the chip is mounted on an RF dunk probe and tested in a screen room intended to shield the digital circuit from ambient RF noise. We immersed the probe in 4.2 K liquid helium. This measurement setup contained attenuators at room temperature to reduce noise on the chip with values of 20 dB on the input signal line and 56 dB on the bias line. This setup is comparable to the CFR setup of Fig. 1 (C), but we save the detailed comparison until the discussion section. We sent a square wave to the input converter and a DC bias to each converter, and on-chip resistors converted bias voltages to currents. We measured the output signal through a 2.5 MHz low-pass filter followed by a 1 -MHz bandwidth preamplifier. To reduce reflections from the filter before the preamplifier, we added a 3 dB attenuator at the filter input. Fig. 2 (B) shows the input and output waveforms, where the output waveform is shown after dividing by the preamplifier's gain. The output waveform frequency is half of the input waveform frequency and the waveforms are synchronized. This behavior indicates the creation of an SFQ in a JTL and a corresponding detection event on every input clock cycle.

Following that, we conducted tests on the LJJs in the DP. For this, we use the previously described launcher and setup.

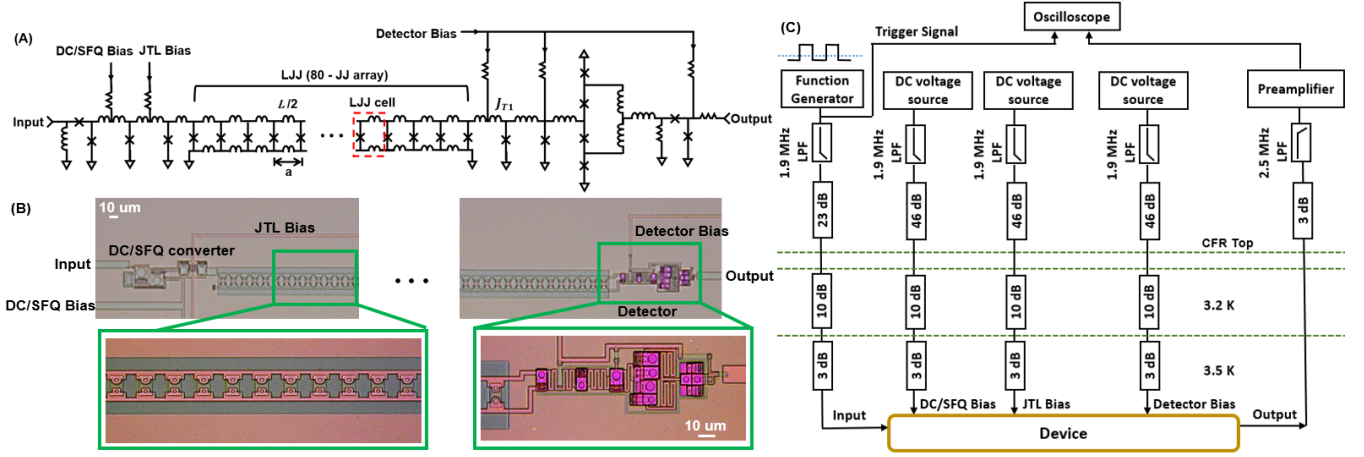


Fig. 1. The engineered LJJ test circuit. (A) The circuit diagram shows the DC/SFQ launcher, the LJJ, and the detector circuit. The LJJ is comprised of 80 JJs and many inductors of value $L/2$. Each cell of the LJJ has length a and total inductance L . (B) Optical photographs of the fabricated circuit featuring enlarged detail of the discrete LJJ cells and the detector. The LJJ has two long rails of inductors (analogous to ladder rails) and an array of JJs and vias, which connect the rails like rungs on a ladder. The JJs have a critical current of $7.5 \mu\text{A}$. The detector is an SFQ/DC converter that includes a two-JJ JTL stage at its input. The JJs have a critical current of approximately $20 \mu\text{A}$. Along with some bias at the end of the LJJ, this JTL stage is intended to power the fluxon further into a T flip-flop. The detector's JJs are five times smaller than that of the JJs on the launcher (DC/SFQ converter). In the optical photographs, the green areas near the LJJ show holes in the ground plane underneath the LJJ. (C) A schematic drawing of the CFR measurement setup is shown; the DP setup was comparable (see main text). A 3 dB attenuator is inserted before the preamplifier's high-impedance input to reduce reflections back to the detector.

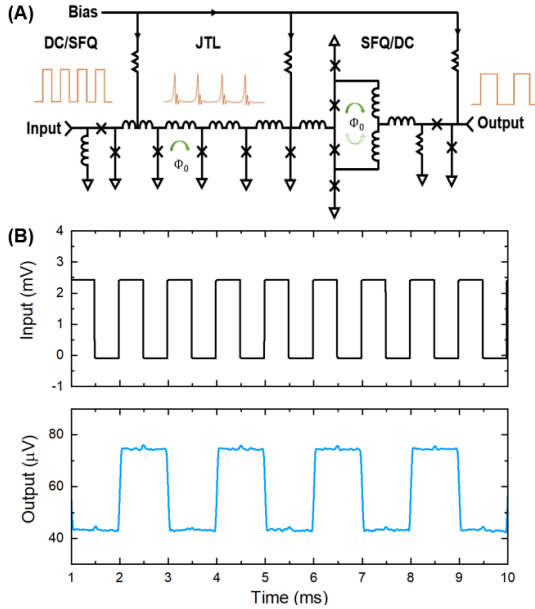


Fig. 2. A reference DC/SFQ and SFQ/DC converter circuit without LJJs. (A) Circuit schematic. The circuit includes a DC/SFQ converter that generates SFQ pulses. These pulses are injected into a short JTL and then detected by an SFQ/DC converter. The JJs in this circuit have a critical current of approximately $100 \mu\text{A}$. The bias currents are set at roughly 75% of the critical current of the Josephson junctions, providing sufficient amplitude to trigger the junctions in response to an incoming SFQ pulse. The central element of the SFQ/DC converter is a T flip-flop, which changes state when it receives an SFQ pulse. After a second SFQ, the circuit toggles back to its initial state. Therefore, two periods of the input waveform should produce one period in the output waveform. (B) Test result from a 1 kHz input waveform (upper panel) shows the proper operation of the converter circuitry in our DP setup (lower panel).

The launcher was made to send SFQ through JTL sections with JJ critical currents of $100 \mu\text{A}$. However, the JJs in our LJJ have a nominal critical current $I_C = 7.5 \mu\text{A}$, and the center portion of half of the fluxon energy is stored within a couple of JJs of the LJJ, resulting in the fluxon energy being lower than that of a SFQ made from $100 \mu\text{A}$ JTL sections. We must use a detector with JJs that are much smaller. Thus we chose JJs that are five times smaller for our fluxon detection circuit than our launcher and the previously mentioned converter.

We measured the output waveform for the LJJ in its test circuit, which yielded an amplitude of approximately $50 \mu\text{V}$. Data was taken up to 1 MHz input frequency, with representative data shown in Fig. 3. As the input frequency increases, the preamplifier's 1 MHz maximum bandwidth filters the high harmonics of the output square wave, causing the output to appear similar to a sinusoidal waveform. By counting the number of periods of the output data, we found that the output frequency was half of the input frequency, indicating that fluxons passed through the LJJ. However, this LJJ test has a relatively high variation in the time between transitions (higher jitter) than the converter-only test. We will discuss the jitter more after showing results from the other setup on the same initial chip.

C. Measurement of LJJs with the CFR setup

The same initial chip was then installed on the CFR. The CFR setup is shown in Fig. 1 (C). This setup has 13 dB of attenuation at low temperature on all input lines, with a 23 dB attenuator at room temperature on the input signal line, and 46 dB attenuator at room temperature on the bias lines. Additionally, the setup has a 1.9 MHz low-pass filter on input lines to lower noise.

Similar to the DP, we measured the DC output in the CFR setup (see Fig. 4). Again we find the setup's capability of operating

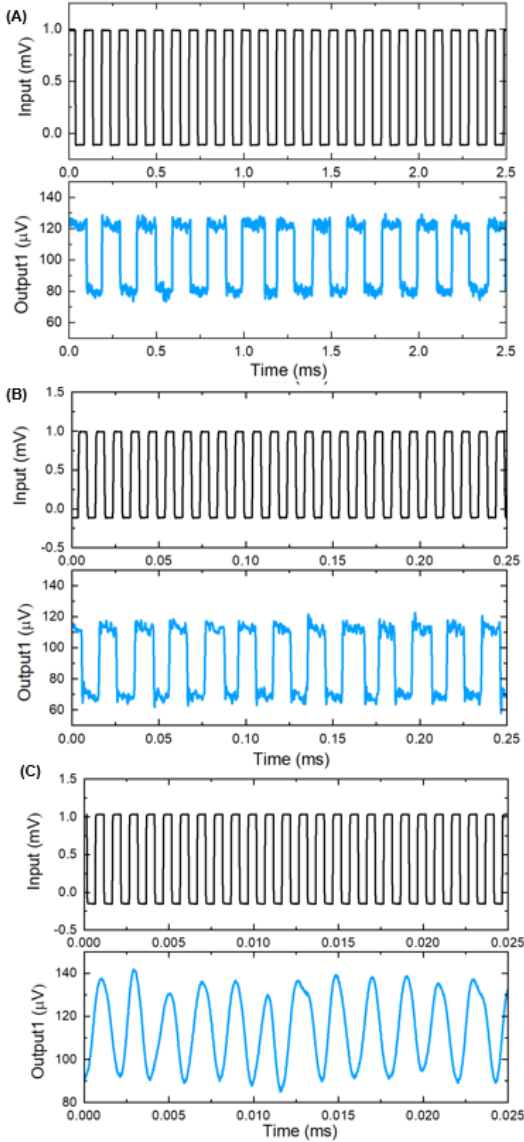


Fig. 3. LJJ test-circuit data taken with the DP setup, shown with the corresponding input waveforms. (A), (B), and (C) show the converter output voltage for input fluxon frequencies of 10 kHz, 100 kHz, and 1 MHz, respectively. Similar to the circuit in Fig. 2, due to the operation of the output converter, the output frequency is half of the input frequency. At low frequencies, the output amplitude is approximately $50 \mu\text{V}$.

at frequencies as high as 1 MHz. The output amplitude is approximately $65 \mu\text{V}$ at low frequencies. The difference in output amplitude between the two setups is due to a different bias value applied to the detector. Similar to the DP setup, the preamplifier's 1 MHz bandwidth smooths the output signal waveform and lowers the amplitude at 1 MHz.

The operation margins of 10 kHz input signal amplitude, DC/SFQ bias, input JTL bias, and detector bias (see Fig. 1) are 23.4%, 18.25%, 11.57%, and 8.7%, respectively. Input-to-output crosstalk is observed (shown in Fig. 4), but we have not yet determined the cause. Compared to the results obtained from the DP setup, the data here exhibit a relatively stable pulse width (low jitter), indicating that the CFR provides a lower noise environment for the circuit than the DP. For some

unknown reason, the jitter is worse at the low frequency of 10 kHz than at the higher frequencies of 100 kHz and 1 MHz (see Appendix B). The input and output filtering contribute to the narrowing of the eye-opening as frequency increases (as shown in Appendix B).

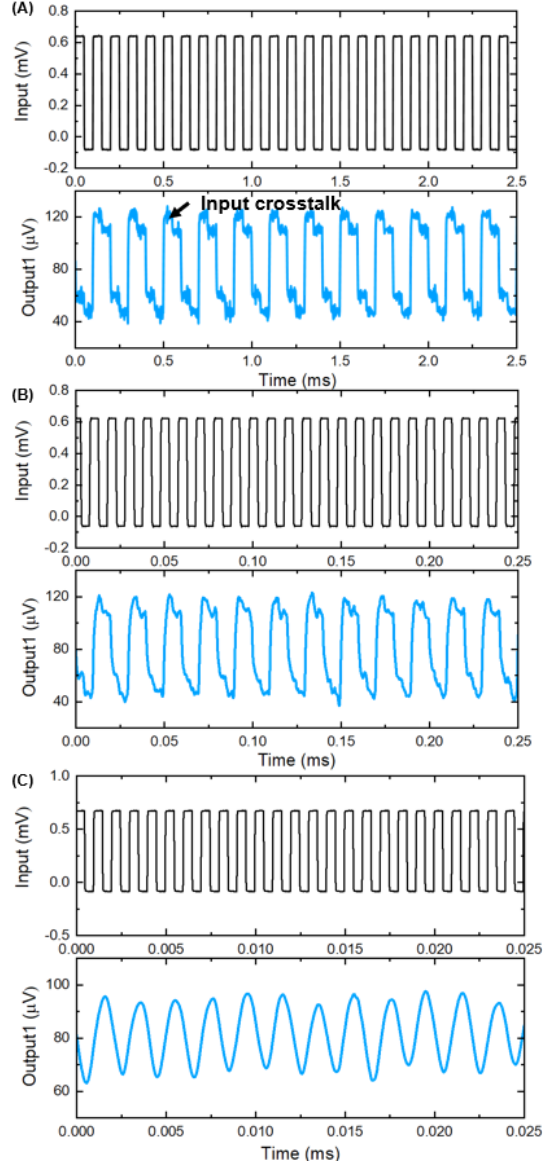


Fig. 4. LJJ test-circuit data taken with the CFR setup, shown with the corresponding input waveforms. (A), (B), and (C) show the converter output at operating frequencies of 10 kHz, 100 kHz, and 1 MHz, respectively. Input-to-output crosstalk is observed at the lowest frequency. At 1 MHz, the arrival of the input waveform at the chip and the output waveform from the chip are attenuated by input and output filters. The output-line filtering transforms the 1 MHz square wave nearly into a sine wave. As expected, the output frequency is half of the input signal frequency. The output amplitude at low frequency is approximately $65 \mu\text{V}$.

D. Discussion

In our engineered LJJs, the rest energy of a fluxon is $E_{FL}(v=0) = 8I_C\Phi_0\lambda_J/2\pi a \approx 47 \text{ zJ}$, where Φ_0 is the flux quantum. The ballistic gates of RFL were optimized with fluxons carrying 20% of kinetic energy [26], corresponding

to a fluxon velocity $v = 0.6c$, and giving total fluxon energy of $E_{FL}(v = 0.6c) = 10I_C\Phi_0\lambda_J/2\pi a \approx 59$ zJ. However, when simulating the circuit of Fig. 1 (A), we find that the fluxons are launched from the DC/SFQ converter at higher speed, with $v = 0.78c$, and kinetic energy to rest energy ratio of $1/\sqrt{(1-0.78^2)} - 1 = 60\%$. The energy loss for a stopped fluxon (possibly from an LJJ defect) is 0.6×47 zJ ≈ 30 zJ. The fluxons could have been stopped in the LJJs by many effects. However, the fluxon arrival events at the detector indicate the fluxons may have traveled under the power of their own momentum, and the energy loss is smaller than 28 zJ.

According to simulations with discrete LJJs, our fluxons at a speed of $v = 0.78c$ would experience a fractional energy loss of 10^{-3} within a period of v_J^{-1} , where $v_J = \sqrt{I_c/2\pi\Phi_0C_J} = 44$ GHz is the Josephson frequency and $C_J = 300$ fF. At this loss rate, we calculate a 3% energy change for a travel distance of 2060 μm and a time of 682 ps. Our calculated fluxon energy loss is on the order of 1 zJ when traversing our 1300 μm -long LJJ. We intended to achieve lower discreteness than what is currently fabricated in our LJJ. Additionally, post-fabrication, we discovered that our launch velocity would be much larger than the typical simulated value of $v \approx 0.6c$. The combination of these two effects results in an increase in the calculated loss by approximately three orders of magnitude [26]. Therefore, there is potential to significantly reduce the loss in the LJJ if the discreteness and the launch velocity are smaller.

When comparing two setups, the CFR and DP, and the same chip (at nearly the same temperature), both setups exhibit a similar maximum operating frequency. However, the CFR setup exhibits a much lower jitter. This is likely due to much lower environmental noise in the CFR setup than in the DP setup. The most obvious difference between the setups is that 13 dB of the total input attenuation is utilized at low temperatures of the CFR setup, whereas this attenuation is absent in the DP setup. Moreover, the output lines of both setups have low filtering and attenuation, which may cause a noise limitation. Fig. 5 shows the jitter in timing observed in the two measurement setups. This jitter was quantified as the difference in times between transitions of the output waveform at 10 kHz. Recall that the rising and falling transitions in the output waveform indicate the arrival of a fluxon at the output converter. These times are then compared to the input pulse rising times to determine the duration between input pulse generation and output pulse detection. The total signal transfer times encompass filters, converter delays, and fluxon travel time. Both setups demonstrate an electrical delay of approximately 2 μs . The MHz filters in the setup contribute predominantly to this 2 μs electrical delay. The CFR setup exhibits a much narrower standard distribution, indicating low-jitter fluxon arrival events and ballistic fluxon transfer. This study suggests that adding low-temperature filtering to the inputs of our chip could reduce the jitter in the DP setup.

The output waveform in the reference converter circuit which contains no LJJ, had less jitter. Thus, the converter JJs with a critical current that is five times smaller for our LJJ tests, or the 1300 μm -long LJJ renders this circuit more susceptible to environmental noise than the reference converter circuit. Since the LJJ is connected to a different converter

circuit than our reference converter circuit, we can not yet determine if the LJJ or the converter causes higher jitter in our LJJ test circuit.

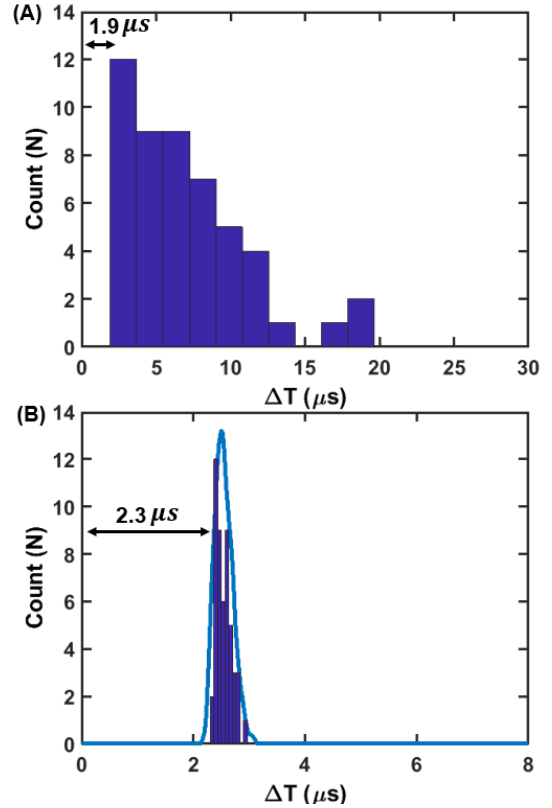


Fig. 5. (A, B) Distribution of time delays between the rising edge of the input waveform and rising and falling edges in the output waveform (containing jitter information). The data of both setups are analyzed for an operating frequency of 10 kHz. In both setups, there is a 2 μs minimum delay magnitude caused by the electrical delay of the input and output filters. (A) Time delay distribution in the DP setup. A wide distribution suggests that the LJJ is causing a delay and is sensitive to the environment (see main text). (B) Time delay distribution in the CFR setup. The Gaussian distribution is fit with a standard deviation of $\sigma = 0.14$ μs . The relatively narrow distribution suggests an improved measurement environment for the LJJ compared to the DP setup. This narrow distribution indicates proper ballistic transfer, contrasting with the wide distribution observed in the DP setup.

III. CONCLUSION

We investigate the motion of fluxons in engineered long Josephson junctions, which can be used as components of ballistic logic gates. The fluxons are analogs to particles due to the nature of the fluxon in the sine-Gordon equation. In our discrete LJJ, they cause the coordinated evolution of JJs. At the beginning of the study, we estimated the discreteness of the LJJ from its measured rail inductance and nominal Josephson junction inductance. Our measurements demonstrate the generation, transmission, and detection of low-energy sine-Gordon fluxons. In both setups, we measured fluxon arrival events at the proper rate. These measurements are consistent with ballistic fluxon transfer. We also analyzed the jitter of fluxon arrival times and found a much lower jitter in the CFR setup. This is likely because the CFR setup provides a significantly improved environment for the fluxons traveling in

the LJJ compared to the DP setup. The detector composed of small critical current JJ may also have been adversely affected by the environment in both setups compared to the reference converter, although we were unable to measure this separately.

The fluxons must be reasonably spaced to minimize interactions, but the upper limit in frequency is on the order of the Josephson frequency ($\nu_J=44$ GHz). However, due to the limitations of our preamplifier and other filtering in our setup, we can currently only measure arriving fluxons at a rate of up to ≈ 1 MHz.

In the study, we calculated the expected energy loss from our structure. Based on the simulated launch velocity of the fluxons and calculations of loss due to plasma wave generation caused by the discreteness of the LJJ, we obtain a realistic estimate for the fluxon energy loss. The cell JJ to linear inductance ratio L_J/L used in this paper is slightly smaller than the planned value of 7. Additionally, our simulations indicate that our fluxon launching speed from the DC/SFQ converter is higher than the standard gate simulation velocity of $0.6c$. Both factors contribute to a much higher energy loss rate from discreteness than necessary. In the future, we plan to decrease the cell inductance L to reduce the loss and obtain parameter margins for our LJJ. This LJJ study shows progress toward using LJJs as necessary gate components in reversible computing.

ACKNOWLEDGMENT

The authors would like to express gratitude to M. P. Frank and R. Lewis for providing the SFQ reference converter chip for testing our measurement setup prior to LJJ testing. The authors also acknowledge scientific interactions with I. Vernik, A. F. Kirichenko, and D. Yohannes from SEEQC (www.seeqc.com) and thank B. Palmer, B. Butera, and C. Richardson from LPS for related scientific interactions.

APPENDIX A SQUID MEASUREMENTS

To explore the inductance properties of a structure similar to the rail on our LJJs, we utilized an SQUID with electrodes to directly inject flux bias current into the SQUID strip line. The inductance can be determined by observing the magnetic field response of the SQUID to the injected flux bias current I_{fl} . When a current I_{fl} is directly injected into the shared strip line, each additional magnetic flux quantum coupled to the SQUID equals the product of ΔI_{fl} and the self-inductance of the shared strip line, where the ΔI_{fl} is the period observed in the SQUID voltage modulation under variation of the flux bias current I_{fl} . Therefore, the self-inductance is given by the flux quantum Φ_0 divided by ΔI_{fl} .

In Fig. 6 (A), we present photographs of the test SQUID. It was cooled in the DP setup and statically biased with a constant current just above the critical current. Fig. 6 (B) and (C) show examples of voltage responses to the flux bias current for two identical design SQUIDs. The self-inductance per μm was extracted using the formula $L_s = (\Phi_0/\Delta I_{fl})/l$, where l represents the length of the shared strip line. From these tests, we obtained an average inductance per μm is 0.654 pH/ μm with a standard deviation of 3.8%.

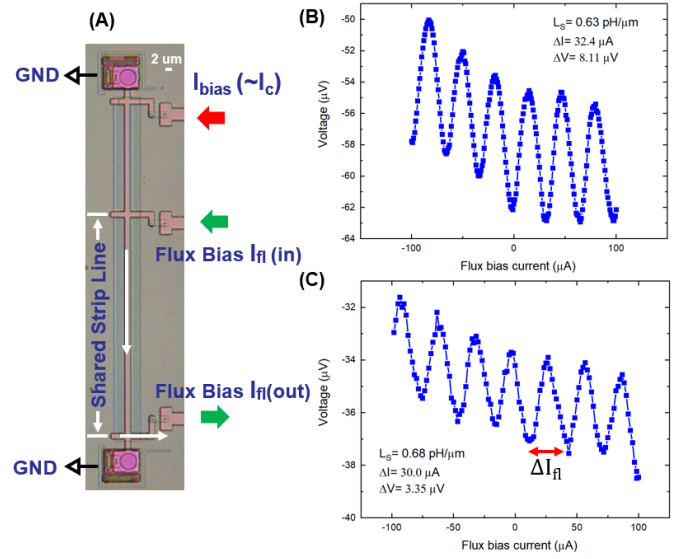


Fig. 6. SQUID test data taken with the DP setup. (A) Optical photograph of Nb SQUID fabricated on the same wafer. (B) and (C) are the characteristics of voltage-injected flux bias current of two identical design SQUIDs on two chips from the same wafer.

APPENDIX B EYE DIAGRAMS

The oscilloscope was used to analyze jitter and eye diagrams. The eye diagram is a visual representation of the signal sliced up and overlaid to show multiple time intervals in the signal, and may influence the bit error rate. Fig. 7 displays the eye diagram of the output signal under the CFR setup, obtained from an oscilloscope with input frequencies of 10 kHz, 100 kHz, and 1 MHz. The number of unit intervals overlaid on the eye diagram for analysis is 3.8 k, 19.6 k, and 73.3 k. The signal undergoes attenuation by a 3 dB attenuator and is then amplified by the preamplifier with a gain of 2000, resulting in an approximate overall amplification factor of 1678. The cross-talk behavior is observed in the middle of the waveform, indicated by the break in the solid line at 10 kHz.

APPENDIX C OUTPUT AMPLITUDE

Fig. 8 shows the circuit schematic between the LJJ detector output and the room temperature electrical components. The LJJ detector output serves as the voltage source. A low-noise voltage preamplifier, with a gain of 2000 and an input impedance of 100 M Ω , conditions the converter output. The dividing factor for the detector output V_{source} compared to the preamplifier input V_{input} is: $V_{\text{input}} = V_{\text{source}} \times \frac{141.99\Omega}{(141.99 + 8.55 + 2.73 + R_{JJ})\Omega} = 0.84V_{\text{source}}$. R_{JJ} represents the internal impedance of the voltage source, which is equivalent to the impedance of the detector's output resistance, estimated to be approximately 16 Ω . V_{input} equals the measured amplified value divided by the gain. Using this, we extract the proper scaling factor between the oscilloscope's voltage and the detector's output voltage.

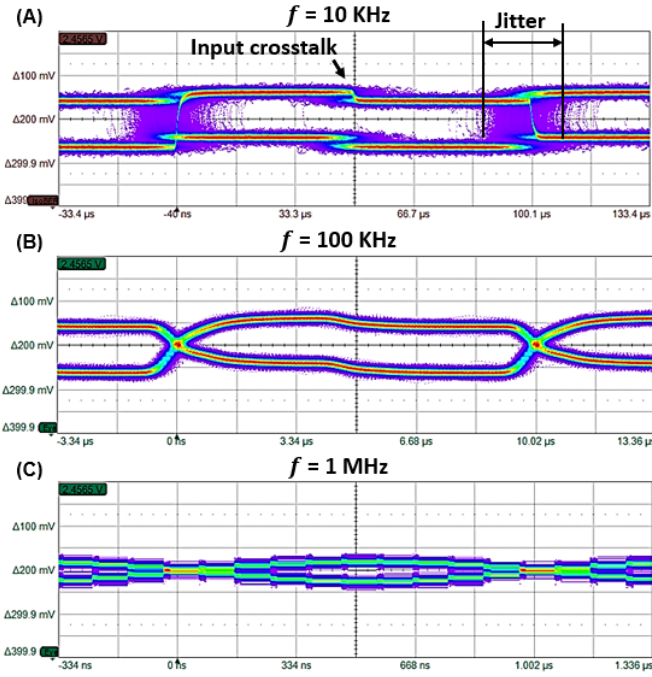


Fig. 7. Eye diagram data captured on an oscilloscope in the CFR setup. The distinguishability of the SFQ/DC converter lowers as the frequency increases to 1 MHz. Jitter at low frequency is explained in the main text.

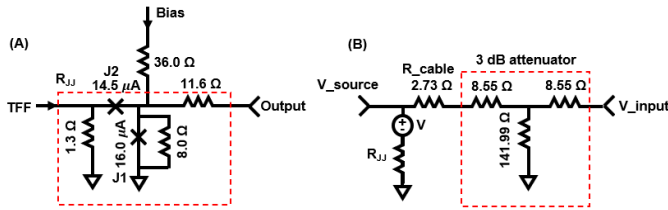


Fig. 8. (A,B) Output circuit schematics. (A) The schematic of the detector output. The junctions utilized in the detector output have an approximate critical current of $15 \mu\text{A}$. (B) The connection circuit at room temperature. R_{cable} includes the chip-probe contact resistance and the cable resistance. R_{JJ} corresponds to the detector impedance, which functions as the internal impedance of the voltage source (V_{source}). V_{input} represents the input voltage of the preamplifier, which input impedance is high.

REFERENCES

- [1] Shalf, John, Sudip Doshanj, and John Morrison. "Exascale computing technology challenges." In High Performance Computing for Computational Science—VECPAR 2010: 9th International conference, Berkeley, CA, USA, 2010, Revised Selected Papers 9, pp. 1-25. Springer Berlin Heidelberg, 2011.
- [2] Burroughs CJ, Dresselhaus PD, Rufenacht A, Olaya D, Elsbury MM, Tang YH, Benz SP. NIST 10 V programmable Josephson voltage standard system. IEEE Transactions on Instrumentation and Measurement. 2011;60(7):2482-8.
- [3] Donnelly CA, Flowers-Jacobs NE, Brevik JA, Fox AE, Dresselhaus PD, Hopkins PF, Benz SP. 1 GHz waveform synthesis with Josephson junction arrays. IEEE Transactions on Applied Superconductivity. 2019;30(3):1-1.
- [4] Kirichenko DE, Filippov TV, Gupta D. Microwave receivers with direct digitization. In 2009 IEEE MTT-S International Microwave Symposium Digest 2009 (pp. 1449-1452). IEEE.
- [5] Kameda Y, Yoroza S, Hashimoto Y, Terai H, Fujimaki A, Yoshikawa N. High-speed demonstration of single-flux-quantum cross-bar switch up to 50 GHz. IEEE transactions on applied superconductivity. 2005;15(1):6-10.
- [6] A. Sahu, M. E. Çelik, D. E. Kirichenko, T. V. Filippov and D. Gupta, "Low-Power Digital Readout Circuit for Superconductor Nanowire

- Single-Photon Detectors," in IEEE Transactions on Applied Superconductivity, vol. 29, no. 5, 1301306 (2019), doi: 10.1109/TASC.2019.2895051.
- [7] Ortlepp T, Hofherr M, Fritzsche L, Engert S, Ilin K, Rall D, Toepfer H, Meyer HG, Siegel M. Demonstration of digital readout circuit for superconducting nanowire single photon detector. Optics Express. 2011;19(19):18593-601.
- [8] Leman, S.W.; Golden, E.B.; Guyton, M.C.; Ryu, K.K.; Semenov, V.K.; Wynn, A. Integrated Superconducting Transition-Edge-Sensor Energy Readout (ISTER). IEEE Trans. Appl. Supercond. 2023, 33, 2500807.
- [9] Çelik ME, Filippov TV, Kirichenko D, Habib M, Talalaevskii A, Sahu A, Gupta D. 25-GHz operation of ERSFQ time-to-digital converter. IEEE Transactions on Applied Superconductivity. 2021;31(5):1-5.
- [10] Bozbey A, Miyajima S, Akaike H, Fujimaki A. Single-flux-quantum circuit based readout system for detector arrays by using time to digital conversion. IEEE transactions on applied superconductivity. 2009;19(3):509-13.
- [11] Leonard Jr E, Beck MA, Nelson J, Christensen BG, Thorbeck T, Howington C, Opremcak A, Pechenezhskiy IV, Dodge K, Dupuis NP, Hutchings MD. Digital coherent control of a superconducting qubit. Physical Review Applied. 2019;11(1):014009.
- [12] Zhang H, Chakram S, Roy T, Earnest N, Lu Y, Huang Z, Weiss DK, Koch J, Schuster DL. Universal fast-flux control of a coherent, low-frequency qubit. Physical Review X. 2021;11(1):011010.
- [13] McDermott R, Vavilov MG. Accurate qubit control with single flux quantum pulses. Physical Review Applied. 2014;2(1):014007.
- [14] Mukhanov OA. Energy-efficient single flux quantum technology. IEEE Transactions on Applied Superconductivity. 2011;21(3):760-9.
- [15] Tanaka M, Ito M, Kitayama A, Kouketsu T, Fujimaki A. 18-GHz, 4.0-aJ/bit operation of ultra-low-energy rapid single-flux-quantum shift registers. Japanese Journal of Applied Physics. 2012; 51(5R):053102.
- [16] Herr QP, Herr AY, Oberg OT, Ioannidis AG. Ultra-low-power superconductor logic. Journal of applied physics. 2011;109(10).
- [17] Dorojevets M, Chen Z, Ayala CL, Kasperek AK. Towards 32-bit energy-efficient superconductor RQL processors: The cell-level design and analysis of key processing and on-chip storage units. IEEE Transactions on Applied Superconductivity. 2014;25(3):1-8.
- [18] Kirichenko DE, Sarwana S, Kirichenko AF. Zero static power dissipation biasing of RSFQ circuits. IEEE Transactions on Applied Superconductivity. 2011;21(3):776-9.
- [19] Semenov VK, Danilov GV, Averin DV. Negative-inductance SQUID as the basic element of reversible Josephson-junction circuits. IEEE transactions on applied superconductivity. 2003;13(2):938-43.
- [20] Takeuchi N, Yamanashi Y, Yoshikawa N. Measurement of 10 zJ energy dissipation of adiabatic quantum-flux-parametron logic using a superconducting resonator. Applied Physics Letters. 2013;102(5).
- [21] Ren J, Semenov VK. Progress with physically and logically reversible superconducting digital circuits. IEEE transactions on applied superconductivity. 2011;21(3):780-6.
- [22] Ayala CL, Tanaka T, Saito R, Nozoe M, Takeuchi N, Yoshikawa N. MANA: A monolithic adiabatic iNtegration architecture microprocessor using 1.4 zJ/op superconductor Josephson junction devices. In 2020 IEEE Symposium on VLSI Circuits 2020 (pp. 1-2). IEEE.
- [23] Takeuchi N, Yamanashi Y, Yoshikawa N. Thermodynamic study of energy dissipation in adiabatic superconductor logic. Physical Review Applied. 2015 ;4(3):034007.
- [24] Takeuchi N, Ehara K, Inoue K, Yamanashi Y, Yoshikawa N. Margin and energy dissipation of adiabatic quantum-flux-parametron logic at finite temperature. IEEE transactions on applied superconductivity. 2012 ;23(3):1700304-1700304.
- [25] Takeuchi N, Yamanashi Y, Yoshikawa N. Simulation of sub-kBT bit-energy operation of adiabatic quantum-flux-parametron logic with low bit-error-rate. Applied Physics Letters. 2013 Aug 5;103(6).
- [26] Wustmann W, Osborn KD. Reversible fluxon logic: Topological particles allow ballistic gates along one-dimensional paths. Physical Review B. 2020 ;101(1):014516.
- [27] Osborn KD, Wustmann W. Reversible fluxon logic with optimized CNOT gate components. IEEE Transactions on Applied Superconductivity. 2020 ;31(2):1-3.
- [28] Osborn KD, Wustmann W. Asynchronous reversible computing unveiled using ballistic shift registers. Physical Review Applied. 2023 ;19(5):054034.
- [29] Frank MP. Asynchronous ballistic reversible computing. In 2017 IEEE International Conference on Rebooting Computing (ICRC) 2017 (pp. 1-8). IEEE.
- [30] Frank MP, Lewis RM, Missert NA, Wolak MA, Henry MD. Asynchronous ballistic reversible fluxon logic. IEEE Transactions on Applied Superconductivity. 2019 ;29(5):1-7.

- [31] Braun OM, Kivshar YS. Nonlinear dynamics of the Frenkel–Kontorova model. *Physics Reports*. 1998 ;306(1-2):1-08.
- [32] Polonsky SV, Semenov VK, Bunyk PI, Kirichenko AF, Kidiyarov-Shevchenko AY, Mukhanov OA, Shevchenko PN, Schneider DF, Zinoviev DY, Likharev KK. New RSFQ circuits (Josephson junction digital devices). *IEEE transactions on applied superconductivity*. 1993 ;3(1):2566-77.
- [33] Pfeiffer J, Abdumalikov Jr AA, Schuster M, Ustinov AV. Resonances between fluxons and plasma waves in underdamped Josephson transmission lines of stripline geometry. *Physical Review B*. 2008 ;77(2):024511.
- [34] Yu L, Wustmann W, Osborn KD. Experimental designs of ballistic reversible logic gates using fluxons. In 2019 IEEE International Superconductive Electronics Conference (ISEC) 2019 (pp. 1-3). IEEE.